Journal of Atmospheric and Solar-Terrestrial Physics 72 (2010) 890–899

Contents lists available at ScienceDirect

Journal of Atmospheric and Solar-Terrestrial Physics

journal homepage: www.elsevier.com/locate/jastp

Effects of the inclusion of bending-to-stretching transitions in the non-LTE modeling of ozone vibrational temperatures

Rafael P. Fernandez [a,*,1], Martin Kaufmann [b], Beatriz M. Toselli [a]

[a] INFIQC, Centro Láser de Ciencias Moleculares, Departamento de Físico Química, Facultad de Ciencias Químicas, Universidad Nacional de Córdoba, 5000 Córdoba, Argentina
[b] Research Center Jülich, Institute for Chemistry and Dynamics of the Geosphere, Jülich, Germany

ARTICLE INFO

Article history:
Received 18 December 2009
Received in revised form
28 April 2010
Accepted 2 May 2010
Available online 11 May 2010

Keywords:
Bending-to-stretching k_{2D} transitions
Vibrational energy transfer
Ozone non-LTE
Collisional k_{VT} rate constants
SSH theory

ABSTRACT

A description of the non-LTE intramolecular ozone relaxation cascade considering the relative importance of different transitions on the $O_3(v_1v_2v_3)$ vibrational levels has been studied by quantifying the kinetic law of every process and transition that affect each level population. The analysis considers the inclusion for the first-time of bending-to-stretching (k_{2D}) transitions in the energy relaxation cascade of ozone after it is formed by three-body recombination. In this way, the vibrational temperatures and the relative contribution of every transition are presented as a function of altitude. The results show that the inclusion of the bending-to-stretching transitions in the O_3 non-LTE relaxation scheme decreases the v_2-mode overpopulation and therefore the stretching levels' population increases, as required for a correct radiance simulation of the 4.8 μm ozone emission in the upper atmosphere.

1. Introduction

The importance of ozone in the atmosphere has been highlighted elsewhere (Brasseur and Solomon, 1984). Its formation in the upper atmosphere proceed through the three-body recombination of atomic and molecular oxygen to produce vibrationally excited $O_3(v_1v_2v_3)$,

$$O_2+O+M\xrightarrow{k_{CP}}O_3(v_1v_2v_3)+M. \quad (1)$$

The excess energy released in the process (1) is deposited in the thermal bath only when $O_3(v_1v_2v_3)$ is deactivated by collisions (Rawlins and Armstrong, 1987; Rawlins et al., 1987; Mlynczak and Drayson, 1990a, b), and consequently the efficiency of heat deposition depends on the competition between collisional quenching processes

$$O_3(v_1'v_2'v_3')+M\xrightarrow{k_{VT}}O_3(v_1v_2v_3)+M, \quad (2)$$

and emission of radiation

$$O_3(v_1'v_2'v_3')\xrightarrow{A_{i,j}}O_3(v_1v_2v_3)+h\nu. \quad (3)$$

At low altitudes, a high collision frequency maintains a Boltzmann vibrational energy distribution characterized by the local kinetic temperature, while at high altitudes, the collision frequency is low and collisions are no longer the sole means of maintaining vibrational distributions because chemical reactions

$$O_3(v_1v_2v_3)+O\xrightarrow{k_{CL}}2O_2 \quad (4)$$

and absorption of light

$$O_3(v_1v_2v_3)+h\nu\xrightarrow{B_{i,j}\,L_{A\nu}}O_3(v_1'v_2'v_3') \quad (5)$$

are also important. Thus, there is a transition from local thermodynamic equilibrium (LTE) at lower altitudes, where collisions are rapid, to non-LTE at higher altitudes, where radiative and chemical processes cannot be neglected (López-Puertas and Taylor, 2001). In these regions, the $O_3(v_1v_2v_3)$ population deviates from the Boltzmann population, and consequently it is necessary to define the vibrational temperature of each independent level,

$$T_{v_1v_2v_3}=\frac{E_{O_3}(v_1v_2v_3)}{k\ln[n_{O_3}(000)/n_{O_3}(v_1v_2v_3)]}, \quad (6)$$

which is different from the local kinetic temperature T_{kin} (Wintersteiner et al., 1992; Edwards et al., 1993; López-Puertas and Taylor, 2001).

The modeling of non-LTE limb spectra of ozone for the different bands has been extensively studied. For example, the 9.6 μm band was modeled for the MIPAS instrument (Manuilova et al., 1998) and the SABER instrument (Mlynczak and Zhou, 1998). Most of the models calculate the vibrational populations by solving a steady state equation including chemical, collisional and radiative processes for ozone and by considering line-by-line radiative transfer at least for the fundamental bands. Recently,

* Corresponding author. Tel.: +54 261 5243000; fax: +54 261 5244531.
E-mail address: rfernandez@fcq.unc.edu.ar (R.P. Fernandez).
[1] Present address: CONICET, Grupo de Estudios Atmosféricos y Ambientales, Secretaría de Ciencia, Tecnología y Posgrado, Facultad Regional Mendoza, Universidad Tecnológica Nacional, 5500 Mendoza, Argentina.

1364-6826/$ - see front matter © 2010 Elsevier Ltd. All rights reserved.
doi:10.1016/j.jastp.2010.05.005

non-LTE corrections have been also applied to the 14.6 and 4.8 μm band emissions retrieval (Gil-López et al., 2005; Kaufmann et al., 2006, respectively). In the last case, the authors suggest decreasing the k_{D2} collisional rate constant by a factor of 3–4 to fit their simulations to the measured radiance. The strong impact that collisional rate constants have on the non-LTE ozone retrieval has already been reported (Mlynczak and Zhou, 1998; Steinfeld and Gamache, 1998).

In this paper, we present a description of the ozone relaxation cascade in the middle atmosphere using different relaxation schemes. The system is solved using a non-LTE model previously presented and validated (Fernandez et al., 2009, hereafter referred as paper I).

2. Ozone energy transfer mechanism

The mechanism used in this study includes processes (1)–(5) as detailed in paper I.

2.1. Chemical processes

The rate constant for ozone chemical production process (1) has been determined precisely by Hippler et al. (1990), and the value $k_{CP}(T)=6.0\times10^{-34}\ (T/300)^{-2.3}$ cm^6 s^{-1} included in the model is independent of the collider. Several nascent vibrational distributions have been proposed (Rawlins and Armstrong, 1987; Rawlins et al., 1987; Mlynczak and Drayson, 1990a, b; Kaufmann et al., 2006), varying from those which promote the population of the lower levels (zero surprisal) to those which populate only the higher levels close to the dissociation threshold (see López-Puertas and Taylor, 2001 or Goussev, 2002 for a detailed discussion). In this work, a narrow single-level nascent distribution centered at $O_3(006)$ level has been used. This selection was based on the findings of von Rosenberg and Trainor (1975) and Kleindienst and Bair (1977), who suggested that 50–70 % of the exothermicity appears as vibrational excitation, mainly in the ν_3-mode (see Kaufmann et al., 2006). Also, according to Barker (2001), the vibrational energy distribution is likely to be relatively narrowed and centered close to the dissociation limit because a broad vibrational energy distribution would require unrealistically high rotational energies in order to satisfy energy conservation.

The O_3+O collisions can proceed through two different reaction channels: the collisional quenching deactivation (2) and the chemical loss reaction (4) that produce excited $O_2(\upsilon)$. The reactive channel contributes at most 30% to the overall O_3+O deactivation (West et al., 1978), with a rate constant (k_{CL}) dependent on the internal ozone energy distribution. Manuilova et al. (1998) have suggested using a fixed value for the fundamental stretching levels and to perform a simple scaling for the higher stretching levels considering only the amount of energy in ν_3-mode. To relate the high energy levels' reactivity to the fundamental rate constant (k^0_{CL}) and to the global rate constant measured for both channels (1.5×10^{-11} cm^3 s^{-1}, West et al., 1976, 1978), the following scaling was implemented in the model:

$$k_{CL}=\begin{cases} k^0_{CL}=8.0\times10^{-12}\ \text{cm}^3\ \text{s}^{-1}, & \text{for}\quad O_3(001)\quad\text{and}\quad O_3(100)\\ \dfrac{5}{7}E_{v3}\dfrac{1.0\times10^{-14}}{1.5\times10^{-11}}k^0_{CL}, & \text{for}\quad O_3(v_1v_2v_3),\ v_1+v_3\geq2\\ & E_{v3}=v_3\times1042\ \text{cm}^{-1}\end{cases} \tag{7}$$

Although there is not rationale to neglect the chemical loss for the bending energy levels, most ozone non-LTE models neglect this pathway (see Manuilova et al., 1998; Mlynczak and Zhou, 1998; Goussev, 2002; Kaufmann et al., 2006). In order to compare our results with the previous ones we decided not to present results including the chemical loss for the bending mode.

2.2. Radiative processes

The band Einstein coefficient of spontaneous emission (A_{ij}) for process (3) has been calculated by means of the HITRAN 2004 molecular spectroscopic database (Rothman et al., 2005). All ozone hot bands are optically thin throughout the whole atmosphere, so the absorption of radiation between layers ($B_{ij}\ L_{\Delta\nu}$) is only considered for the fundamental bands.

2.3. Collisional processes

Vibration-to-translation (VT) transitions are the main energy transfer processes in the lower and middle atmosphere. Several studies have been performed to determine the k_{VT} rate constant values for these processes and their temperature dependence (Ménard-Bourcin et al., 1990, 1991, 1994; Doyennette et al., 1990, 1992; Ménard et al., 1992; Upschulte et al., 1994). Complete descriptions of the kinetics of ozone have also been given (Mlynczak and Drayson, 1990a; Steinfeld and Gamache, 1998). A brief description of the different types of transitions is given in the next section.

3. Collisional transition types

In order to implement the collisional coupling between all ozone vibrational levels in the relaxation scheme, it is necessary to distinguish between the fundamental transitions measured experimentally and the hot transitions. The four fundamental transitions described in the literature are (Fig. 1):

- $O_3(100)\leftrightarrow O_3(001)$ or *intermode* ($\nu_1\leftrightarrow\nu_3$) transition ($\Delta E=61$ cm^{-1}), with a resonant rate constant k^0_r. Here, one vibrational quantum is transferred between modes ν_3 and ν_1. Coriolis-coupling prevents these modes to be treated independently and are usually considered as members of an undistinguishable dyad ($O_3[\nu_D,\nu_2]$, with $\nu_1+\nu_3=\nu_D=1$ and $\nu_2=0$).
- $O_3(100)-O_3(001)\rightarrow O_3(010)$ or ($\nu_{1,3}\rightarrow\nu_2$) *stretching-to-bending* transitions ($\Delta E=341-402$ cm^{-1}). Because these transitions

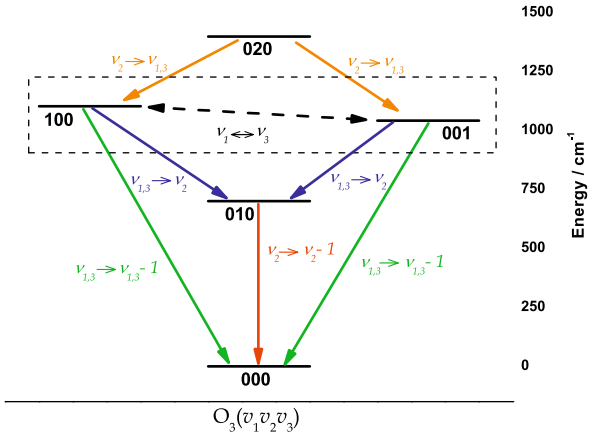

Fig. 1. Vibrational levels of ozone (horizontal lines) and their quantum numbers versus vibrational energy (in cm^{-1}). The first dyad is represented by the dashed rectangle. The arrows represent different types of fundamental collisional VT transitions: $\nu_1\leftrightarrow\nu_3$ coupling, pure-stretching $\nu_{1,3}\rightarrow(\nu_{1,3}-1)$, pure-bending $\nu_2\rightarrow(\nu_2-1)$ and stretching-to-bending $\nu_{1,3}\rightarrow\nu_2$. The proposed $\nu_2\rightarrow\nu_{1,3}$ bending-to-stretching channel is also shown.

are far from resonance, their rate constants (k^0_{D2}) are two orders of magnitude smaller than k^0_r.

- $O_3(010) \rightarrow O_3(000)$ or $(v_2 \rightarrow v_2 - 1)$ *pure-bending* transition ($\Delta E = 701\ cm^{-1}$), where only one energy quantum is transferred from the v_2-mode to the translational degrees of freedom. The k_{VT} rate constant for this type of transition is referred to as k^0_2. Its absolute value is of the same order of magnitude as k^0_{D2}.
- $O_3(100) - O_3(001) \rightarrow O_3(000)$ or $(v_{1,3} \rightarrow v_{1,3} - 1)$ *pure-stretching* transitions ($\Delta E = 1042 - 1103\ cm^{-1}$). The rate constant is referred to as k^0_D and their absolute values are at least one order of magnitude smaller than k^0_2 or k^0_{D2}.

For $O_3 + M$ collisions ($M = N_2$, O_2 and O_3), the temperature dependent equations for $k^0_{D2}(T)$ and $k^0_2(T)$ were taken from Ménard et al., (1992), while an adjusted value of $k^0_D(T)$ was used following Martin Torres (1999). The $k^0_r(T)$ resonant rate constant was taken from Doyennette et al. (1990). The measured values of West et al. (1976, 1978) were used for $O_3 + O$ fundamental transitions (see Manuilova et al., 1998). The fundamental rate constant expressions for collisional transitions included in the model are shown in Table 1.

3.1. Energy scaling

Fig. 2 shows the ozone collisional transitions as a function of the energy level up to 4000 cm^{-1}. For transitions between high energy levels, only Ménard-Bourcin et al. (1994, 1996) have derived absolute rate constants. Then, for hot transitions the individual k^v_{VT} rate constants must be calculated by means of some theory or scaled by a rule. Because of the enormous amount of transitions at high energies, an incorrect scaling factor will expand rapidly in the system.

The Landau–Teller (LT) scaling law (Lambert, 1977) allows the calculation of k^v_{VT} by considering only the total number of stretching or bending quanta on each of the energy levels involved in the transition (Schwartz et al., 1952; Kaufmann et al., 2006). In this way, k^v_2 and k^v_D rate constants scale linearly with v_2 and $v_{1,3}$, respectively, while k^v_r and k^v_{D2} scale with the

Table 1
Fundamental collisional rate constants $k^0_{VT}(T)$ expressions for the different transitions and colliders included in the model.

Collider	N_2	O_2	O_3	O atom	Scaling factor
k^0_r	$1.19 \times 10^{-11} \left(\frac{300}{T}\right)^{0.8}$	$0.97 \times 10^{-11} \left(\frac{300}{T}\right)^{0.7}$	$6.68 \times 10^{-11} \left(\frac{300}{T}\right)^{0.4}$	0	$v_1 v_1 \times (v_3 + 1)$
k^0_{D2}	$1.2 \times 10^{-13} T^{1/2} \exp\left(-\frac{26.8}{T^{1/3}}\right)$	$0.5 \times 10^{-13} T^{1/2} \exp\left(-\frac{22.8}{T^{1/3}}\right)$	$0.7 \times 10^{-13} T^{1/2} \exp\left(-\frac{18.0}{T^{1/3}}\right)$	9.3×10^{-12}	$v_{1,3} \times (v_2 + 1)$
k^0_2	$7.0 \times 10^{-13} T^{1/2} \exp\left(-\frac{40.0}{T^{1/3}}\right)$	$59.0 \times 10^{-13} T^{1/2} \exp\left(-\frac{53.8}{T^{1/3}}\right)$	$5.0 \times 10^{-13} T^{1/2} \exp\left(-\frac{33.0}{T^{1/3}}\right)$	3×10^{-12}	v_2
k^0_D	$3.1 \times 10^{-15} \sqrt{\frac{T}{300}}$	$3.1 \times 10^{-15} \sqrt{\frac{T}{300}}$	$1.06 \times 10^{-14} \sqrt{\frac{T}{300}}$	0	$v_{1,3}$

Units are in $cm^3\ s^{-1}$. The scaling factors for the different transition types are also shown.

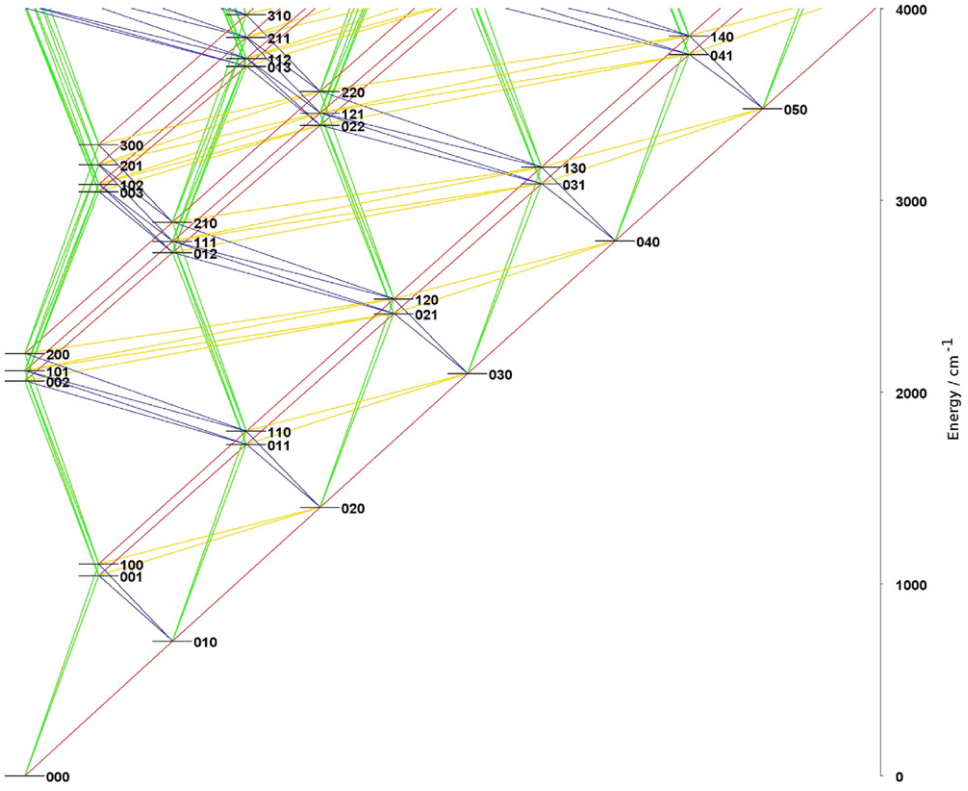

Fig. 2. Vibrational levels of ozone up to 4000 cm^{-1} (horizontal lines) and their quantum numbers versus vibrational energy (in cm^{-1}). The lines represent the different types of fundamental and hot transitions (see previous caption for reference).

Table 2
SSH theory derived values of $k^0_{2D}(T)$ for different colliders.

Collider	N_2	O_2	O_3	Scaling factor
k^0_{2D}	$1.3\times10^{-14}\,T^{1/2}\exp\left(-\frac{26,8}{T^{1/3}}\right)$	$7.0\times10^{-15}\,T^{1/2}\exp\left(-\frac{22,8}{T^{1/3}}\right)$	$1.1\times10^{-14}\,T^{1/2}\exp\left(-\frac{18,0}{T^{1/3}}\right)$	$v_2\times(v_{1,3}+1)$

Units are in $cm^3\,s^{-1}$. The scaling factor for hot transitions is also shown.

product of the quantum numbers changed ($v_1\times[v_3+1]$ and $v_{1,3}\times[v_2+1]$, respectively).

Another way to obtain these rate constants is using the Schwartz, Slawsky and Herzfeld (SSH) semi-classical theory (Schwartz et al., 1952). The SSH theory allows to estimate all transition probabilities considering steric, translational, vibrational and interaction potential adjustable parameters that must be fitted to compare the calculations with the experimental results for the k^0_r, k^0_{D2}, k^0_2 and k^0_D fundamental values (Lambert, 1977). A detailed application of this theory to ozone can be found in Fernandez (2009). Once the fundamental rate constants are adjusted, it is reasonable to assume that the same set of parameters is valid to obtain the excited k^v_{VT}. The advantage of SSH theory lies on the possibility of estimating all transitions probabilities.

3.2. Bending-to-stretching transitions

Considering the fundamental level transitions, the only one that causes energy transference from the bending mode to the stretching levels is the upward stretching-to-bending transition with an inverse rate constant k'_{D2}. Hence, there is no any direct $v_2\rightarrow v_{1,3}$ relaxation channel in the downward direction. This is the reason why once the $O_3(0v_20)$ levels are populated, they will only be able to relax throughout $v_2\rightarrow v_2-1$ pure-bending transitions (Gil-López et al., 2005; Kaufmann et al., 2006; paper I), producing a marked overpopulation of $O_3(0v_20)$ family levels. This fact produces an underestimation of the emitted radiance from the 4.8 μm band in the remote sensing of MIPAS (Kaufmann et al., 2006).

When the $O_3(020)$ level is considered in the analysis, another relaxation channel can be proposed: an $O_3(020)\rightarrow O_3(100)-O_3(001)$ or ($v_2\rightarrow v_{1,3}$) *bending-to-stretching* transition can occur, which exchanges a total of 3 quanta (2 quanta from the bending mode must be lost in order to gain 1 quantum in one of the stretching modes) and releases $296-357\,cm^{-1}$ of energy (see Fig. 1). The fundamental rate constants for these transitions (k^0_{2D}) have been calculated using the SSH theory. Its absolute value is in the same order of magnitude than k^0_D pure-stretching transitions for the 200–300 K temperature range, with a temperature dependence similar to $k^0_{D2}(T)$. These results are not surprising according to the conventional wisdom on energy transfer (Yardley, 1980). Although k^0_{2D} is not exactly a fundamental rate constant, this is the lowest downward bending-to-stretching transition, and therefore it should be used as the fundamental transition reference to perform the scaling for hot transitions. Table 2 shows $k^0_{2D}(T)$ for different colliders derived from SSH theory. The LT scaling factor used to obtain excited k^v_{2D} rate constants is $v_2\times(v_{1,3}+1)$. It is important to mention that for O_3+O collisions, a $k^0_{2D}=0$ value has been used.

4. Ozone non-LTE model

The non-LTE model presented in paper I was used for the calculations. Briefly, the structure of the model atmosphere includes 66 non-regularly spaced altitude layers between surface and 120 km constituted by N_2, O_2, O_3, O and H. The pressure, volume mixing ratios and temperature profiles are representative of a typical mid-latitude atmosphere during daytime, even though both day- and night-time conditions can be evaluated providing the O_3 abundance externally. For the ozone molecule, a total of 105 vibrational energy levels up to $E\approx6250\,cm^{-1}$ are considered, including a collisional coupling of levels only by transitions that exchange at most two quanta per mode.

4.1. Kinetics of vibrational levels

The kinetic law for each $O_3(v_1v_2v_3)$ level is

$$\frac{d[O_3(v_1v_2v_3)]}{dt}=k^{\delta i}_{CP}[M][O_2][O]+\left\{\sum_j A^{ij}+\sum_j k^{ij}_{VT}[M]\right\}[O_3(v'_1v'_2v'_3)]-\left\{k^i_{CL}[O]+\sum_j A^{ji}+\sum_j k^{ji}_{VT}[M]\right\}[O_3(v_1v_2v_3)], \tag{8}$$

where the index i accounts for $O_3(v_1v_2v_3)$ level and the index j accounts for any other $O_3(v'_1v'_2v'_3)$ vibrational level. A^{ij} and A^{ji} are the Einstein A coefficients for spontaneous emission and are included either in the production or in the loss terms depending on whether the transition comes from a higher excited state or whether it goes to a lower energy state. In the case of fundamental transitions, A^{ij} and A^{ji} also represent the Einstein B coefficients for stimulated absorption times for the mean radiance of the spectral band $L_{\Delta v}$.

4.2. Relaxation schemes

Three relaxation schemes have been used during this work. First, we have used the same relaxation scheme as the one used in paper I. This is considered as a baseline or *normal* scheme to assess the impact of the inclusion of the new relaxation channel. Second, in the *BTS* scheme, bending-to-stretching transitions were added to the normal scheme. Because the $O_3(0v_20)$ family members are usually overpopulated with respect to the rest of the levels, the contribution that k_{2D} rate constants will make on the kinetic law will be significant compared to the one of k_D. Third, an empirical $k_{D2}/3$ scheme proposed by Kaufmann et al. (2006) was implemented. This scheme was used to fit 4.8 μm radiance simulations to the MIPAS experimental data. It is important to highlight that in the $k_{D2}/3$ case, the LT scaling factor used was empirically divided by 3 so the fundamental k^0_{D2} rate constants remain unaltered.

5. Results and discussion

The description of ozone energy transfer will focus on the $O_3(v_1v_2v_3)$ non-fundamental lower vibrational levels, i.e. $O_3(020)$, $O_3(011)$ and $O_3(002)$, the last one being directly involved in the 4.8 μm radiance emissions of the atmosphere. Transitions affecting the $O_3(010)$, $O_3(001)$ and $O_3(100)$ fundamental levels have been previously presented in paper I. Section 5.1 presents the changes in the vibrational temperature profiles obtained with the

three schemes. In Section 5.2, the deactivation channels are discussed.

5.1. Vibrational temperatures

Fig. 3 shows the vibrational temperatures for the $O_3(020)$, $O_3(011)$ and $O_3(002)$ levels obtained with the normal (T_{vib}^{normal}) and the BTS (T_{vib}^{BTS}) relaxation schemes. The effect of the inclusion of the bending-to-stretching transitions is clearly reflected in the T_{vib} values: the T_{020}^{BTS} profile shows smaller values than T_{020}^{normal}, while T_{011}^{BTS} and T_{002}^{BTS} show greater values than when the normal scheme is used. The departure of the T_{vib}^{normal} profile from T_{kin} occurs in a 3-step sequence as the altitude increases**:** first, the three levels depart from LTE with the same T_{vib} value at 50 km; then, T_{020}^{normal} deviates further from the T_{vib} of the other levels at 55 km; and lastly, a difference between T_{011}^{normal} and T_{002}^{normal} can be observed above 70 km. In contrast, the results obtained from the BTS scheme show that the T_{011}^{BTS} and T_{002}^{BTS} profiles deviate independently from the T_{020}^{BTS} values at all altitudes.

Fig. 3 also shows the vibrational temperature differences between both schemes:

$$\Delta T_{vib}^{BTS} = T_{vib}^{BTS} - T_{vib}^{normal}. \quad (10)$$

Here, the 3-step sequential departure is not observed when the BTS scheme is used: the T_{002}^{BTS} value is different from T_{011}^{BTS} and T_{020}^{BTS} above 50 km. The BTS scheme causes a maximum decrease of $\Delta T_{020}^{BTS} = -13.9$ K at 86 km, while the greatest ΔT_{011}^{BTS} and ΔT_{002}^{BTS} differences are 8.1 K at 86 km and 13.4 K at 72.5 km, respectively. Also up to the altitude of 84 km, the T_{011}^{BTS} values are smaller than T_{002}^{BTS}, while this situation is inversed above this altitude. In this way, the consideration of the BTS scheme does not only reduce the $O_3(020)$ overpopulation, but also distinguishes the initial deviation of the excited stretching levels from T_{kin} according to the dyad/polyad to which they belong (O_3[1,1] and O_3[2,0], respectively).

In order to compare the impact that the simulated T_{vib} would have on the satellite remote sensing, Fig. 3 also shows $\Delta T_{vib}^{k_{D2}/3}$ profiles. Kaufmann et al. (2006) have mentioned that the inclusion of the $k_{D2}/3$ scheme allows to double the simulated radiance for the 4.8 μm emission band at 60 km originated mainly on the $O_3(002)$ and $O_3(101)$ levels. Because the altitude variation of the emitted radiance depends directly on the T_{vib} profiles of the emitting levels, a direct comparison of ΔT_{002}^{BTS} and $\Delta T_{002}^{k_{D2}/3}$ can be performed. As it can be seen in the right panel, the effects produced by both schemes are similar: the ΔT_{002} and ΔT_{011} profiles show positive differences with respect to the normal scheme, while the opposite is observed for pure-bending level. However, the differences obtained from the $k_{D2}/3$ scheme are considerably larger than those from the BTS scheme, principally for $O_3(002)$ level between 55 and 72.5 km. In particular, $\Delta T_{002}^{BTS} = 13.4$ K at 72.5 km, while $\Delta T_{002}^{k_{D2}/3} = 19.1$ K at 67.5 km.

$\Delta T_{vib}^{k_{D2}/3}$ profiles for the stretching levels exceed the profiles for the BTS scheme up to 75–80 km. Above the height of 85 km, $T_{011}^{BTS} > T_{002}^{BTS}$, while this inversion is not evident when the $k_{D2}/3$ scheme is considered. This effect is related to the different ΔT_{020} values between both schemes: within the BTS scheme, the vibrational overpopulation for $O_3(020)$ level decreases significantly ($\Delta T_{020}^{BTS} < -10$ K between 82 and 90 km), provoking a continuous increase of T_{011}^{BTS}; while $\Delta T_{020}^{k_{D2}/3} = -3.7$ K at 75 km and even shifts to positive values above 80 km, which causes an increase of the net amount of energy transference throughout v_2-mode (see next section). In this way, even though the BTS scheme cannot account for the required $O_3(002)$ and $O_3(101)$ population increase to reproduce the emission at 4.8 μm, it accounts for a considerable portion of it. Note that the $k_{D2}/3$ scheme arises as a mere empirical adjustment of the spectra, while the BTS scheme arises as a consequence of an energy transfer analysis for ozone using SSH theory. What is more is that there are several other unknowns and uncertainties which might modify the T_{vib} profiles such as the nascent energy distribution and the neglect of the k_{CL} for the $O_3(0v_20)$ family members.

5.2. Relative contribution of transitions

In the following figures, the contributions of the transitions that increase the population of a specific level are presented with empty symbols, while the contributions that decrease the level population are presented with full symbols. In this way, when the contributions of the most important pairs of opposite transitions

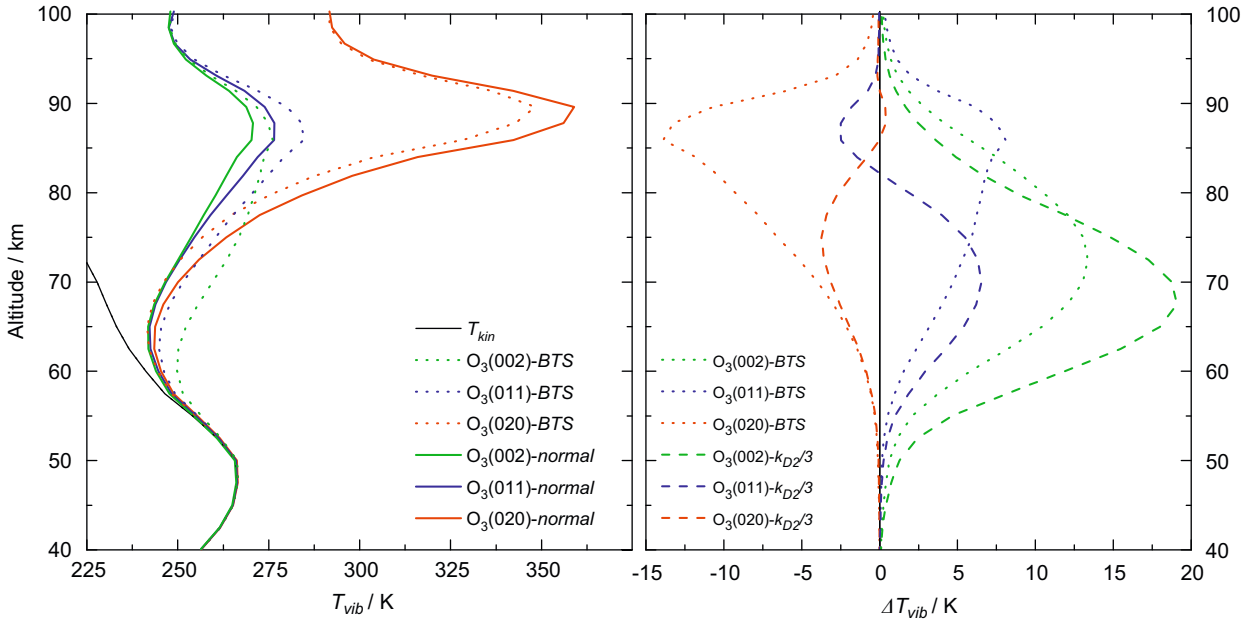

Fig. 3. Vibrational temperatures (T_{vib}) for the $O_3(020)$, $O_3(011)$ and $O_3(002)$ non-fundamental levels as a function of altitude. The right panel presents the ΔT_{vib} differences between the considered relaxation schemes: normal scheme (solid lines), BTS scheme (dotted lines) and $k_{D2}/3$ scheme (dashed lines). T_{kin} is also shown.

are balanced, the level population follows a Boltzmann distribution and LTE prevails. If at least one of them is unbalanced, non-LTE may appear depending on the relative importance of the unbalanced transition as described in paper I.

5.2.1. $O_3(020)$ level

Fig. 4a and b shows the relative contribution to $O_3(020)$ level obtained with the normal (Rel_{normal}) and the BTS (Rel_{BTS}) schemes, respectively. In both cases the direct radiative transitions have a negligible contribution below 75 km, so the non-LTE appearance for this level occurs as a consequence of unbalanced VT processes. The higher pure-bending transitions $O_3(030) \leftrightarrow O_3(020)$ (rhombus symbols) show a notable downward imbalance above 60 km. These transitions cause the non-LTE appearance for $O_3(020)$ level because they are the only unbalanced transition at 50 km when T_{020} deviates from T_{kin}. The lower pure-bending transitions, $O_3(020) \leftrightarrow O_3(010)$, are the most important contributors below 90 km and also show a marked downward imbalance. Therefore, it can be assumed that there is a strong energy relaxation cascade throughout v_2-mode , causing the $O_3(0v_20)$ overpopulation.

In Fig. 4a, note how the stretching-to-bending transitions (triangles symbols) are unexpectedly balanced up to 77.5 km where the upward depopulating transitions surpass the downward. This is unusual because it implies that above this altitude the global effect of the $O_3(011) \leftrightarrow O_3(020)$ [and $O_3(110) \leftrightarrow O_3(020)$] transitions is to produce a net energy transference in the upward direction, which is caused by the $O_3(020)$ overpopulation. In Fig. 4b, these bending-to-stretching transitions are no longer balanced and the unusual upward energy transference is not observed until 85 km is reached. Then, the inclusion of k_{2D} rate constants in the BTS scheme allows the energy that reaches $O_3(0v_20)$ levels to return to the stretching modes, reducing the pure-v_2-mode overpopulation. What is more, the $O_3(020) \rightarrow O_3(001)$ [and $O_3(020) \rightarrow O_3(100)$] bending-to-stretching contributions (square symbols) are comparable to the stretching-to bending transition contributions. In this way, the change from the k_{D2} balanced contributions (Fig. 4a) to the predominant

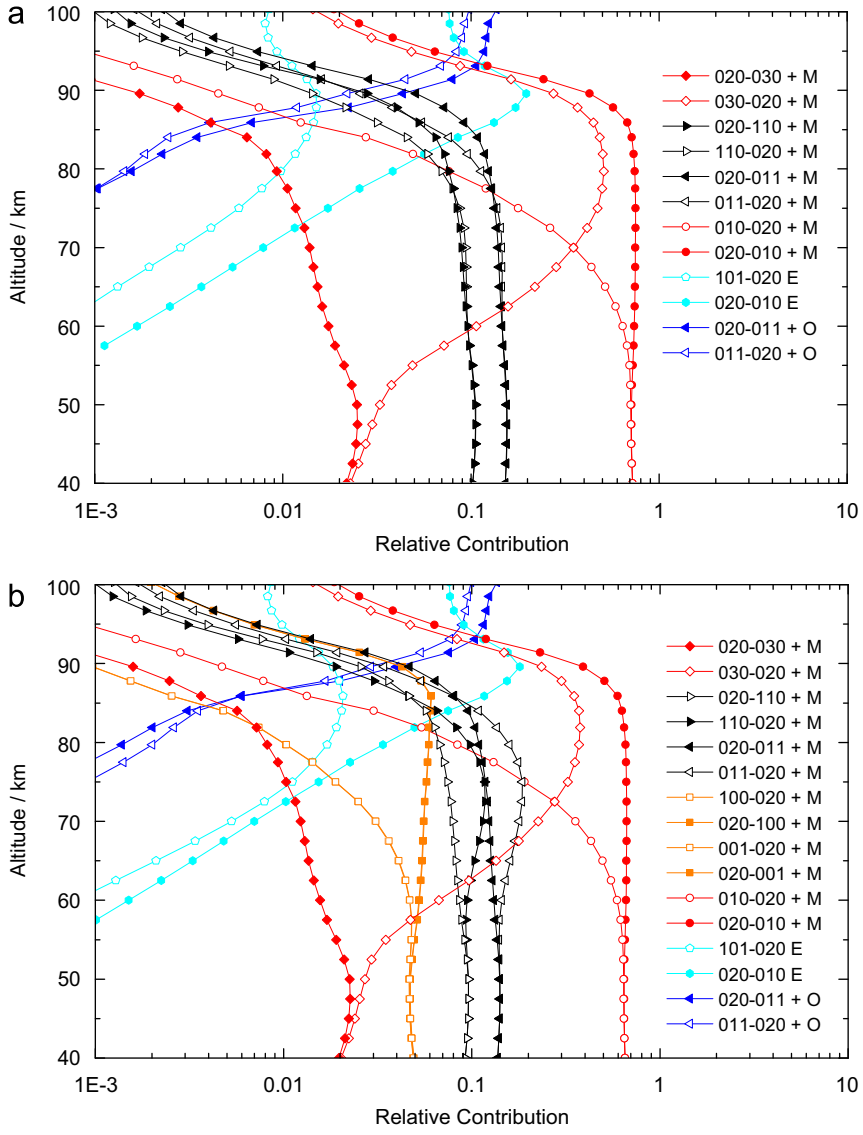

Fig. 4. Relative contribution of transitions populating (empty symbols) and depopulating (filled symbols) $O_3(020)$ level as a function of altitude considering: (a) the normal scheme; and (b) the BTS scheme. The N_2 and O_2 collisional contributions have been added together and referred to as *M*, while *E* stands for Emission. Symbols represent the different types of transitions described in the text: circle (lower pure-bending), pointing left/right triangles (stretching-to-bending), rhombus (higher pure-bending), squares (bending-to-stretching) and pentagon (radiative). The $O_3(020) \rightarrow O_3(001)$ and $O_3(020) \rightarrow O_3(100)$ contributions are superimposed in Fig. 4b.

downward energy transference of k_{D2} transitions (greater values for empty triangles in Fig. 4b) can be attributed to the inclusion of k_{2D} rate constants. Even though the unexpected upward energy transference is also observed for the BTS scheme above 85 km, at this altitude the O_3+O collisions have surpassed the importance of the O_3+M VT processes. Because k_{2D} rate constants have only been included for M=N_2/O_2/O_3 collisions, whenever the contribution of O_3+O collisions surpasses the one for O_3+M, the upward imbalance appears for k_{D2} transitions independently of the type of collider.

The absolute variation of the relative contributions of transitions affecting O_3(020) level for the BTS and the k_{D2}/3 schemes (ΔRel_{BTS} and $\Delta Rel_{k_{D2}/3}$, respectively) are presented in Fig. 5. Similarly to Eq. (10), ΔRel is calculated considering the normal scheme as reference. In the case of the k_{2D} transitions, $\Delta Rel_{BTS} = Rel_{BTS}$.

Fig. 5a shows that the relative contribution of pure-bending transitions for the BTS scheme diminishes as much as 15 % for the $O_3(030) \rightarrow O_3(020)$ transition and 8% for $O_3(020) \rightarrow O_3(010)$ transition. This implies that the O_3(020) overpopulation has decreased because the former populating transition has been reduced by a greater percent than the later depopulating one. This reduction in the dominant energy flux throughout v_2-mode is compensated mainly by the appearance of positive $O_3(020) \rightarrow O_3(001)/O_3(100)$ contributions in the BTS scheme. Even more, the inclusion of the k_{2D} channel also contributes to a further O_3(020) depopulation throughout the reduction in the $O_3(020) \rightarrow O_3(011)$ [and $O_3(020) \rightarrow O_3(110)$] upward contribution (full triangle symbols).

Fig. 5b shows that the contributions for the k_{D2} transitions decrease when the k_{D2}/3 scheme is used. The $O_3(011) \leftrightarrow O_3(020)$ downward contribution has a larger negative variation compared to the upward one, but the differences between opposite transitions are not as marked as in the case of the BTS scheme. Another important difference observed from the k_{D2}/3 scheme is

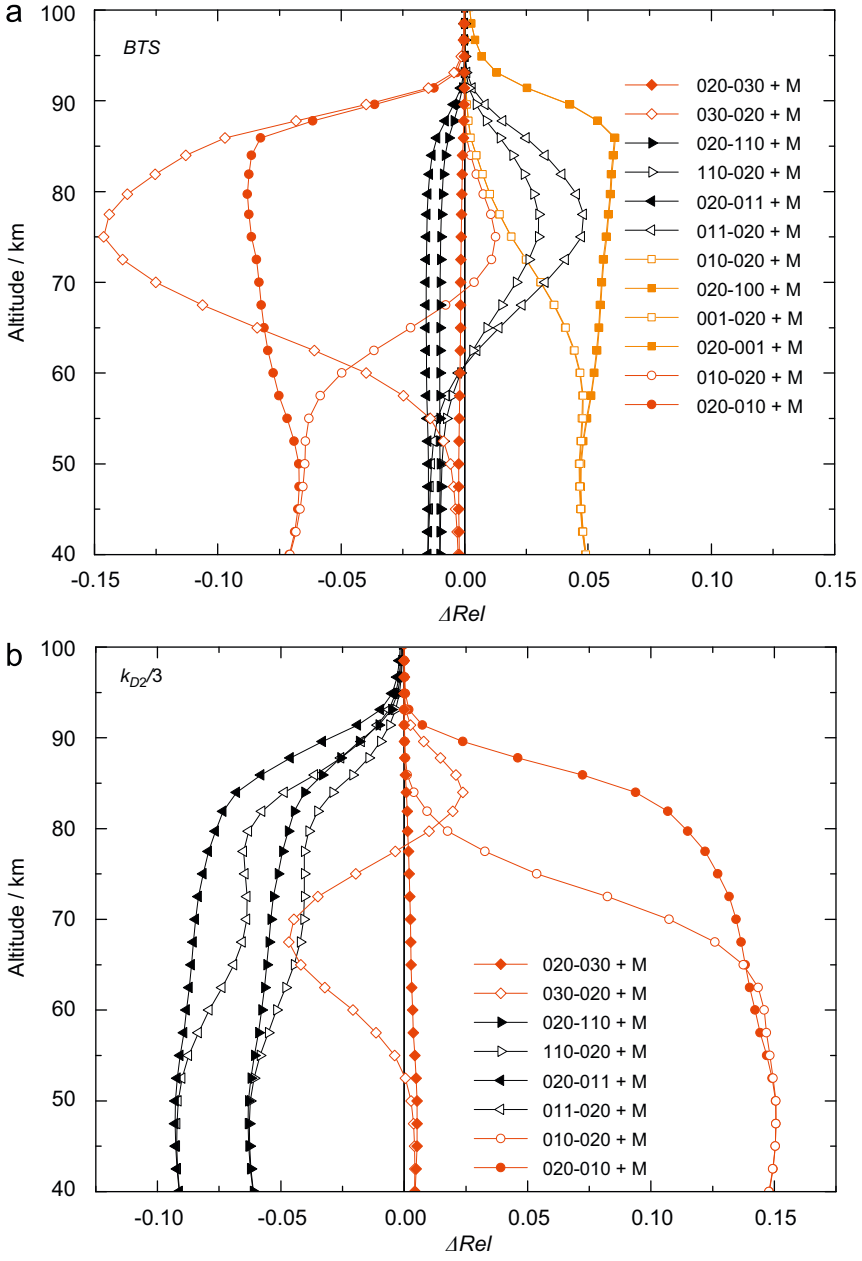

Fig. 5. ΔRel variations of the relative contributions of transitions affecting O_3(020) level between 40 and 100 km considering: (a) the BTS scheme; and (b) the k_{D2}/3 scheme. The symbols reference is detailed in the caption of Fig. 4. The $O_3(020) \rightarrow O_3(001)$ and $O_3(020) \rightarrow O_3(100)$ differences are superimposed in Fig. 5a.

that the $O_3(020) \rightarrow O_3(010)$ pure-bending deactivation increases as much as 15% with respect to the normal scheme, in agreement with a reduction of the $O_3(020)$ overpopulation. But, at the same time, it implies that an even greater portion of the total energy is being transferred throughout v_2-mode. This is consistent with the findings of Kaufmann et al. (2006), who mentioned that an increase in the k_2 rate constant produces a similar effect than the reduction in the value of k_{D2} for O_3[2,0].

5.2.2. $O_3(011)$ level

Fig. 6 shows the Rel_{BTS} contributions and ΔRel_{BTS} variations for the most important transitions affecting $O_3(011)$ level (the results for $O_3(110)$ level are very similar and are not shown). When T_{011}^{BTS} deviates from T_{kin} at 50 km, both $O_3(030) \rightarrow O_3(011)$ and $O_3(021) \rightarrow O_3(011)$ transitions are unbalanced in the downward direction, so the inclusion of k_{2D} rate constants directly affects the appearance of non-LTE. The most important contributions when non-LTE appears are the $O_3(011) \leftrightarrow O_3(020)$ transitions, which between 55 and 85 km show a downward imbalance. Radiative transitions make a significant contribution only above 70 km. The ΔRel_{BTS} variations show that the inclusion of BTS energy transference of $O_3(030) \rightarrow O_3(011)$ transition is partially compensated by a decrease in the $O_3(020) \rightarrow O_3(011)$ upward contribution.

The effects observed when considering the $k_{D2}/3$ scheme are shown in Fig. 7. Here, the contribution of $O_3(011) \leftrightarrow O_3(001)$

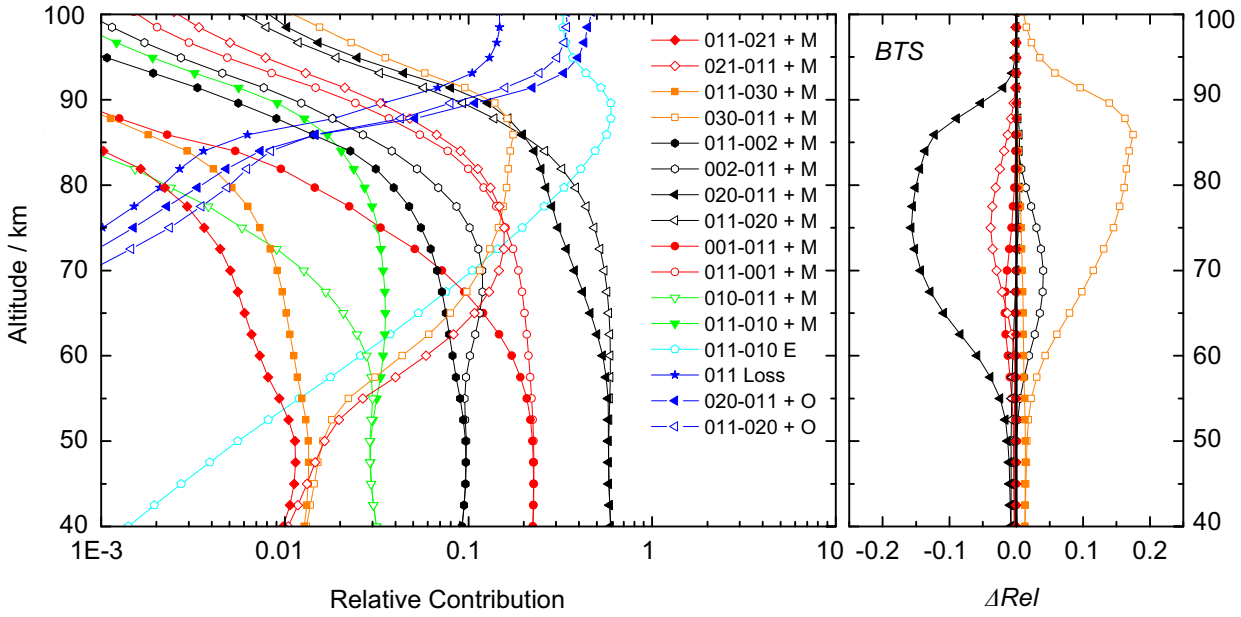

Fig. 6. Relative contribution (left panel) and ΔRel variations (right panel) of the transitions affecting $O_3(011)$ level considering the BTS relaxation scheme. The symbols reference is similar to the one in Fig. 4, but further includes: hexagons (higher stretching-to-bending), pointing down triangles (pure-stretching) and stars (chemical loss).

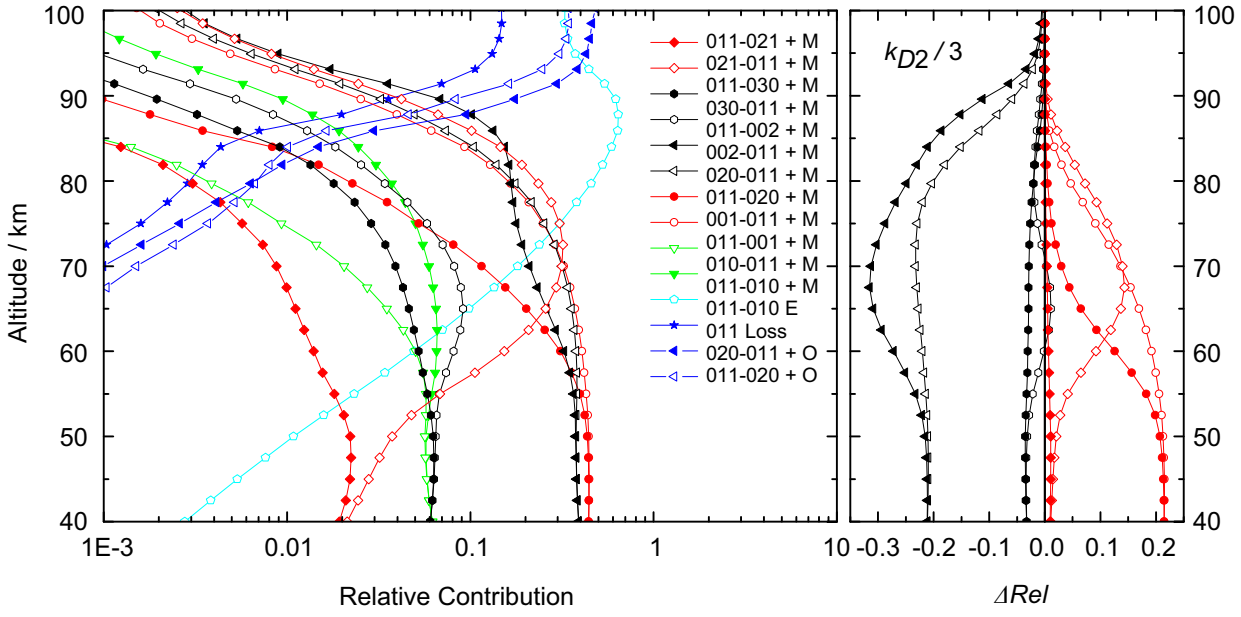

Fig. 7. Idem Fig. 6, but considering the $k_{D2}/3$ relaxation scheme.

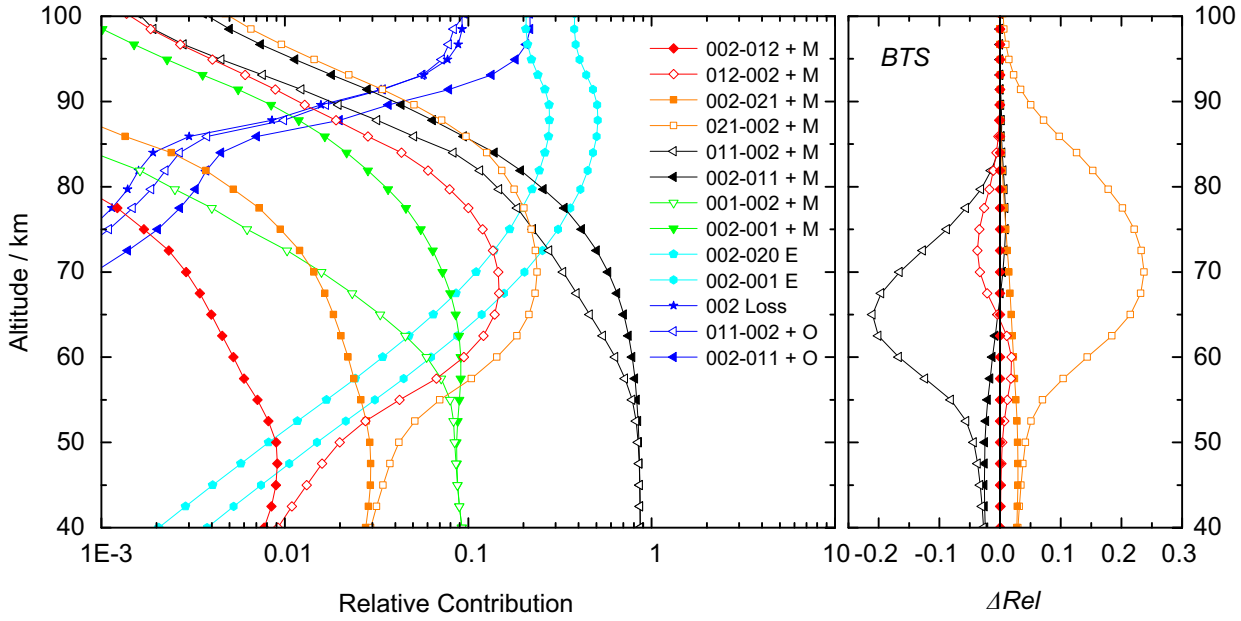

Fig. 8. Idem Fig. 6, but for $O_3(002)$ level. The symbols reference is similar to the one in Fig. 4, but further includes: hexagons (radiative), pointing down triangles (pure-stretching) and stars (chemical loss).

pure-bending transitions are larger than the $O_3(011)\leftrightarrow O_3(020)$ stretching-to-bending transitions, a result not observed before for non-$O_3(0\nu_2 0)$ levels (see paper I). In this case, the appearance of non-LTE is only caused by the imbalance in the $O_3(021)\leftrightarrow O_3(011)$ transitions (rhombus symbols), which becomes the most important contributor at 70 km. The $\Delta Rel_{k_{D2}/3}$ panel also shows that the decrease in importance of k_{D2} transitions is compensated by an increase on the pure-bending contributions, favoring the downward direction. Even though Figs. 6 and 7 show the unusual upward imbalance for k_{D2} transitions, its appearance occurs at 85 km in the BTS scheme and at 80 km with the $k_{D2}/3$ scheme. In both cases, the same inversion can be observed at the same altitude for the O_3+O collisions.

5.2.3. $O_3(002)$ level

The results obtained for $O_3(002)$ level when the BTS scheme is considered are shown in Fig. 8. Similar results are observed for the other members of the O_3[2,0] polyad, which are not shown. When non-LTE appears, the relative importance of the main collisional transitions follow the same behavior as the $O_3(001)$ fundamental level (see paper I). But in this case $O_3(021)\rightarrow O_3(002)$ and $O_3(012)\rightarrow O_3(002)$ transitions rapidly exceed the contribution of the pure-stretching, being the former transitions responsible for the non-LTE appearance of $O_3(002)$ level. The contribution of the k_{2D} downward transition becomes the second most important between 55 and 70 km, which is a consequence of the larger populations of the ν_2-mode rich vibrational levels; $O_3(002)$ level is the last member of the $O_3(040)\rightarrow O_3(021)\rightarrow O_3(002)$ chain within the BTS scheme, receiving part of the $O_3(0\nu_2 0)$ overpopulation.

In this case and unlike the results shown in Fig. 6, the k_{D2} inverse contribution never surpasses the direct one. The 24 % increase of $O_3(021)\rightarrow O_3(002)$ transition at 70 km is once again compensated by a 21 % decrease in the $O_3(011)\rightarrow O_3(002)$ upward stretching-to-bending transition (see right panel), while pure-bending contributions do not vary much.

5.3. Changes in the deactivation cascade

Although both the BTS and the $k_{D2}/3$ schemes produce similar effects on the T_{vib} profiles for the lower excited levels, the correspondent internal energy transference between the different vibrational levels is markedly different. While the $k_{D2}/3$ scheme thermalizes the O_3 molecule less efficiently and increases the energy relaxation flux throughout $v_2\rightarrow v_2-1$ transitions, the BTS scheme favors the energy return from the bending mode to the stretching levels.

Within the BTS scheme, the contribution of bending-to-stretching transitions is not negligible when the appearance of non-LTE for $O_3(011)$ and $O_3(002)$ levels is analyzed. Their contribution is similar to the pure-stretching and pure-bending transition contributions. When the k_{2D} transitions are included, the unusual upward energy transference from the $O_3(020)$ overpopulated level is reduced. For all levels, the positive ΔRel profile for bending-to-stretching transitions is counteracted by a decrease in the relative importance of pure-bending and stretching-to-bending transitions. This implies that at least a portion of the energy that reaches the bending energy levels is being thermalized-back to the stretching modes.

When considering the BTS scheme, apart from the direct contribution of k_{2D} downward transitions, $O_3(011)$ and $O_3(002)$ levels are also indirectly affected through lower energy levels, the upward $O_3(020)\rightarrow O_3(011)$ and $O_3(011)\rightarrow O_3(002)$ stretching-to-bending transitions, respectively. Even though these indirect transitions are also present in the normal scheme, their contributions are considerably different because the starting levels are also affected by another k_{2D} transition. The $O_3(020)$ level can also deactivate through a k_{2D} transition to $O_3(001)$ level (see Fig. 4a), while $O_3(011)$ is also affected by a k_{2D} populating transition from $O_3(030)$ level (see Fig. 6). Also, as the energy level increases, the direct contribution increases faster than the indirect one, which is explained considering that the $O_3(0\nu_2 0)$ overpopulation is larger for high energy levels.

Within the $k_{D2}/3$ scheme, the $v_2\rightarrow v_2-1$ contributions to the relaxation cascade increase for all levels. This increase causes a

dominant downward cascade, throughout the pure-bending channel without promoting an intermode energy exchange. Then, the stationary $O_3(011)$ and $O_3(002)$ populations increase as required for improving the modeling of MIPAS 4.8 μm radiance, but once the energy reaches $O_3(020)$ or any of the $O_3(0\nu_20)$ levels it can no longer return to the stretching levels. Then, with this scheme, the $O_3(\nu_1\nu_2\nu_3)$ populations are more prone to depend on the nascent energy distribution.

6. Concluding remarks

In this work, variations in the non-LTE populations of the $O_3(020)$, $O_3(011)$ and $O_3(002)$ levels when bending-to-stretching transitions are included in the energy transfer mechanism were analyzed. The k_{2D} rate constants included in the BTS scheme were calculated using the SSH theory, assuming that the adjusted vibrational parameters for k^0_{D2}, k^0_2 and k^0_D rate constants can be extended to the unmeasured k^0_{2D}. Also, the most important transitions affecting the appearance of non-LTE for all levels were identified by computing the kinetic law of every process and transition that populate/depopulate each level. In order to analyze the differences between the different relaxations schemes used, the changes in the vibrational population (ΔT_{vib}) and relative contribution (ΔRel) were calculated.

The results presented in Section 5 highlight the importance of including the bending-to-stretching transitions in the energy relaxation mechanisms for ozone. The consideration of the BTS scheme accounts for the increase in $O_3(002)$ level populations as a consequence of allowing the energy that reach $O_3(0\nu_20)$ levels to be transferred back to the stretching modes by VT collisions. The increase observed for ΔT^{BTS}_{002} is comparable to the changes obtained when the empirical $k_{D2}/3$ scheme is used, while the decrease in T_{020} is considerably greater within the BTS scheme. Then, the inclusion of the BTS scheme can account for a considerable portion of the $O_3(002)$ population increase required for the correct adjustment of the 4.8 μm emission detected by MIPAS.

Acknowledgements

The authors would like to thank CONICET, ANPCyT (Préstamo BID PICT 309) and SeCyT (UNC) for partial support for the work reported here. R.P. Fernandez thanks CONICET for the graduate fellowships and DAAD for a research fellowship at Juelich Research Center, Germany. B.M. Toselli thanks Prof. John Barker for providing the original version of the SSH code and for useful discussions. M. Kaufmann would also like to thank B. Funke for fruitful discussions.

References

Barker, J., 2001. Personal Communication.

Brasseur, G., Solomon, S., 1984. Aeronomy of the Middle Atmosphere. D. Reidel Publishing Company, The Netherlands.

Doyennette, L., Ménard, J., Ménard-Bourcin, F., 1990. Coriolis assisted intermode vibrational energy transfers in O_3–M gas mixtures (M=O_2, N_2, Ar) from infrared double-resonance measurements. Chemical Physics Letters 170, 197–200.

Doyennette, L., Boursier, C., Ménard, J., Ménard-Bourcin, F., 1992. $\nu_1 \leftrightarrow \nu_3$ coriolis-assisted intermode transfers in O_3–M gas mixtures (M=O_2 and N_2) in the temperature range 200–300 K from IR double-resonance measurements. Chemical Physics Letters 197, 157–160.

Edwards, D.P., López-Puertas, M., López-Valverde, M.A., 1993. Non-local thermodynamic equilibrium studies of the 15 μm bands of CO_2 for atmospheric remote sensing. Journal of Geophysical Research 98 (D8), 14955–14977.

Fernandez, R.P., Kaufmann, M., Toselli, B.M., 2009. Relative importance of ozone energy transfer processes in the middle and upper atmosphere. Journal of Atmospheric and Solar-Terrestrial Physics 71, 805–815.

Fernandez, R.P., 2009. Modelado del comportamiento del ozono en la alta atmósfera bajo condiciones de no-ETL. Tesis Doctoral, Universidad Nacional de Córdoba-INFIQC, Argentina.

Gil-López, S., López-Puertas, M., Kaufmann, M., Funke, B., García-Comas, M., Koukouli, M.E., Glatthor, N., Grabowski, U., Höpfner, M., Stiller, G.P., von Clarmann, T., 2005. Retrieval of stratospheric and mesospheric O_3 from high resolution MIPAS spectra at 15 and 10 μm. Advances in Space Research 36, 943–951.

Goussev, O., 2002. Non-LTE diagnostics of the infrared observations of the planetary atmosphere. Dissertation an der Fakultät für Physik der Ludwing-Maximilians-Universität, München.

Hippler, H., Rahn, R., Troe, J., 1990. Temperature and pressure dependence of ozone formation rates in the range 1–1000 mbar and 90–370 K. Journal of Chemical Physics 93, 6560–6569.

Kaufmann, M., Gil-López, S., López-Puertas, M., Funke, B., García-Comas, M., Glatthor, N., Grabowski, U., Höpfner, M., Stiller, G.P., von Clarmann, T., Koukouli, M.E., Hoffmann, L., Riese, M., 2006. Vibrationally excited ozone in the middle atmosphere. Journal of Atmospheric and Solar-Terrestrial Physics 68, 202–212.

Kleindienst, T., Bair, E.J., 1977. Vibrational disequilibrium in bulk reaction systems. Chemical Physics Letters 49, 338.

Lambert, J.D., 1977. Vibrational and Rotational Relaxation in Gasses. Clarendon Press.

López-Puertas, M., Taylor, F.W., 2001. Non-LTE Radiative Transfer in the Atmosphere. World Scientific, Singapore.

Manuilova, R.O., Gusev, O.A., Kutepov, A.A., von Clarmann, T., Oelhaf, H., Stiller, G.P., Wegner, A., López-Puertas, M., Martín-Torres, F.J., Zaragoza, G., Flaud, J.-M., 1998. Modelling of non-LTE limb spectra of i.r. ozone bands for the MIPAS space experiment. Journal of Quantitative Spectroscopy and Radiative Transfer 59, 405–422.

Martin Torres, J.F., 1999. Emisiones infrarrojas del ozono en la atmósfera de la Tierra. Tesis Doctoral, Universidad de Granada—Instituto Astrofísico de Andalucía, España.

Ménard, J., Doyennette, L., Ménard-Bourcin, F., 1992. Vibrational relaxation of ozone in O_3–O_2 and O_3–N_2 gas mixtures from infrared double-resonance measurements in the 200–300 K temperature range. Journal of Chemical Physics 96 (8), 5773–5780.

Ménard-Bourcin, F., Doyennette, L., Ménard, J., 1990. Vibrational energy transfer in ozone from infrared double-resonance measurements. Journal of Chemical Physics 92 (7), 4212–4221.

Ménard-Bourcin, F., Ménard, J., Doyennette, L., 1991. Vibrational relaxation of ozone in O_3–O_2 and O_3–N_2 gas mixtures from infrared double-resonance measurements. Journal of Chemical Physics 94 (3), 1875–1881.

Ménard-Bourcin, F., Doyennette, L., Ménard, J., 1994. Vibrational energy transfers in ozone excited into the (101) state from infrared double-resonance measurements. Journal of Chemical Physics 101 (10), 8645–9636.

Ménard-Bourcin, F., Boursier, L., Doyennette, L., Ménard, J., 1996. Vibrational energy transfer in ozone excited to the (101) state: double-resonance measurements and semiclassical calculations in the 200–300 K temperature range. Journal of Physical Chemistry 100, 15015–15020.

Mlynczak, M.G., Drayson, S.R., 1990a. Calculation of infrared limb emission by ozone in the terrestrial middle atmosphere: 1. Source functions. Journal of Geophysical Research 95 (D10), 16497–16511.

Mlynczak, M.G., Drayson, S.R., 1990b. Calculation of infrared limb emission by ozone in the terrestrial middle atmosphere: 2. Emission calculations. Journal of Geophysical Research 95 (D10), 16513–16521.

Mlynczak, M.G., Zhou, D.K., 1998. Kinetic and spectroscopic requirements for the measurement of mesospheric ozone at 9.6 μm under non-LTE conditions. Geophysical Research Letters 25 (5), 639–642.

Rawlins, W.T., Armstrong, R.A., 1987. Dynamics of vibrationally excited ozone formed by three-body recombination. I. Spectroscopy. Journal of Chemical Physics 87 (9), 5202–5208.

Rawlins, W.T., Caledonia, G.E., Armstrong, R.A., 1987. Dynamics of vibrationally excited ozone formed by three-body recombination reaction. II. Kinetics and mechanism. Journal of Chemical Physics 87, 5209.

Rothman, L.S., Jacquemart, D., Barbe, A., Benner, D.C., Birk, M., Brown, L.R., Carleer, M.R., Chackerian, C., Chance, K., Coudert, L.H., Dana, V., Devi, V.M., Flaud, J.M., Gamache, R.R., Goldman, A., Hartmann, J.-M., Jucks, K.W., Maki, A.G., Mandin, J.-Y., Massie, S.T., Orphal, J., Perrin, A., Rinsland, C.P., Smith, M.A.H., Tennyson, J., Tolchenov, R.N., Toth, R.A., Vander Auwera, J., Varanasi, P., Wagner, G., 2005. Journal of Quantitative Spectroscopy and Radiative Transfer 96, 139–204.

Schwartz, R.N., Slawsky, Z.I., Herzfeld, K.F., 1952. Calculation of vibrational relaxation times in gases. Journal of Chemical Physics 20, 1591.

Steinfeld, J.I., Gamache, R.R., 1998. Energy transfer and inelastic collisions in ozone. Spectrochimica Acta, Part A 54, 65–76.

Upschulte, B.L., Green, B.D., Blumberg, W.A.M., Lipson, S.J., 1994. Vibrational relaxation and radiative rates of ozone. Journal of Physical Chemistry 98 (9), 2328–2336.

von Rosenberg, C.W., Trainor, D.W., 1975. Excitation of ozone formed by recombination. Journal of Chemical Physics 63, 5348.

West, G.A., Weston, R.E., Flynn, G.W., 1976. Deactivation of vibrationally excited ozone by $O(^3P)$ atoms. Chemical Physics Letters 42, 488–493.

West, G.A., Weston, R.E., Flynn, G.W., 1978. The influence of reactant vibrational excitation on the $O(^3P_J)+O_3^*$ bimolecular reaction rate. Chemical Physics Letters 56, 429–433.

Wintersteiner, P.P., Picard, R.H., Aharma, R.D., Winick, J.R., Joseph, R.A., 1992. Line-by-line radiative excitation model for the non-equilibrium atmosphere: application to CO_2 15 μm emission. Journal of Geophysical Research 97 (D16), 18083–18117.

Yardley, J., 1980. Introduction to Molecular Energy Transfer.. Academic Press, New York.